ELSEVIER

Marine Geology 215 (2005) 215–236

MARINE GEOLOGY
INTERNATIONAL JOURNAL OF MARINE GEOLOGY, GEOCHEMISTRY AND GEOPHYSICS

www.elsevier.com/locate/margeo

Early diagenesis of magnetic minerals in marine transitional environments: geochemical signatures of hydrodynamic forcing

Daniel Rey*, Kais J. Mohamed, Ana Bernabeu, Belén Rubio, Federico Vilas

Departamento de Geociencias Marinas, Universidad de Vigo, 36310 Vigo, Spain

Received 25 April 2003; received in revised form 11 October 2004; accepted 10 December 2004

Abstract

The low-field magnetic susceptibility (χ) of surficial sediments from the Ria de Pontevedra (NW Spain) shows a characteristic, hydrodynamically driven textural control, where diamagnetic sandy bioclastic carbonates occur toward the coastline, leaving the finer muddy sediments to be deposited in the central and deeper areas of the ria. Three gravity cores were collected from the inner (core 1), middle (core 2) and outer (core 3) zones of the clayey-rich central axis of the ria, from which the magnetic properties, geochemical characteristics and hydrodynamic regime of the uppermost 90 cm of the sediment record were reconstructed. χ profiles have a distinctive pattern that is controlled by depth. Isothermal remanent magnetization (IRM) acquisition curves facilitated the identification of three well-defined zones with depth, depending on their degree of magnetic saturation, and thus of their dominant magnetic behaviour: magnetite-like, goethite-like and greigite-like. This zonation is interpreted as the result of mineralogical changes during early diagenesis. The relative depths of each zone are mostly dependent on distance to the open sea, with the magnetite-like zones being thicker in the outermost part of the ria. Toward the inner part of the ria, the three zones become shallower and thinner. In the innermost areas, only greigite-like coercivities are observed. Good correlation between magnetic and geochemical parameters such as χ vs. 2Fe/S, or H_{cr} vs. C/S, demonstrates that magnetic property variations with depth are diagenetically controlled, and that these parameters can be used as magnetic proxies for early diagenesis. Similar significant positive correlations were found between χ of the clay fraction and modelled wave heights, and between other magnetic and hydrodynamic parameters, providing magnetic evidence of cryptic wave climate forcing of the diagenetic pathway. The combined analysis of the magnetic, geochemical and hydrodynamic data ultimately indicates that the sediment distribution and subsequent diagenetic pathway in this type of transitional environment mostly depend on the local distribution of wave energy and water depth, rather than on estuarine-like circulation processes.

Keywords: subtidal sediments; magnetic properties; early diagenesis; hydrodynamic forcing; geochemistry; Galician rias

* Corresponding author. Tel.: +34 986 812 004; fax: +34 986 812 556.
E-mail address: danirey@uvigo.es (D. Rey).

0025-3227/$ - see front matter © 2004 Elsevier B.V. All rights reserved.
doi:10.1016/j.margeo.2004.12.001

1. Introduction

Measurement of the magnetic properties of marine sediments has long been established as a useful tool for the study of diagenetic changes in marine environments. The importance of these studies relies on their capability to identify the extent to which diagenetically driven changes in the magnetic mineralogy may hamper the interpretation of palaeomagnetic and rock magnetic data (Thompson and Oldfield, 1986; Verosub and Roberts, 1995; Dekkers, 1997; Evans and Heller, 2004). Magnetic properties also hold valuable information of their own. The post-depositional evolution of most marine sediments depends upon their organic matter content, sedimentation rate, bottom water oxygenation and degree of mixing in the upper sediment layer (Karlin, 1985, 1987; Canfield and Berner, 1987; Leslie et al., 1990; Robinson, 2000; Robinson and Sahota, 2000; Larrasoaña et al., 2003). These sediment features will ultimately determine whether or not suboxic conditions become established in the sediment, during which the continuous process of bacterially mediated organic matter remineralization results in transformation and dissolution of magnetic iron oxides (Karlin and Levi, 1983; Karlin, 1990; Bloemendal et al., 1992; Dekkers, 1997; Passier et al., 1998; Frederichs et al., 1999; Roberts et al., 1999; Robinson et al., 2000; Yamazaki et al., 2003; Liu et al., 2004; Funk et al., 2004; Emiroglu et al., 2004).

Transitional coastal environments in areas of seasonal upwelling, like the Galician Rias Baixas on the NW coast of Spain, typically have very high rates of sedimentation (1–3 mm yr^{-1}) and organic matter supply (Rubio et al., 2001), thus intense diagenesis occurs during early burial under conditions ranging from oxic to suboxic–sulphidic (after Berner, 1981). In contrast with more widely studied continental shelf and deep marine environments where diagenesis is mostly controlled by diffusion of oxygen from oxic bottom waters into the sediment (Jago and Jones, 2002; Scourse and Austin, 2002; Jouanneau et al., 2002), the diagenetic pathway in ria environments mostly depends on the local water depth, distribution of wave energy along the shore area and subsequent sediment texture distribution, and on the degree and frequency of seabed remobilization. Given similar

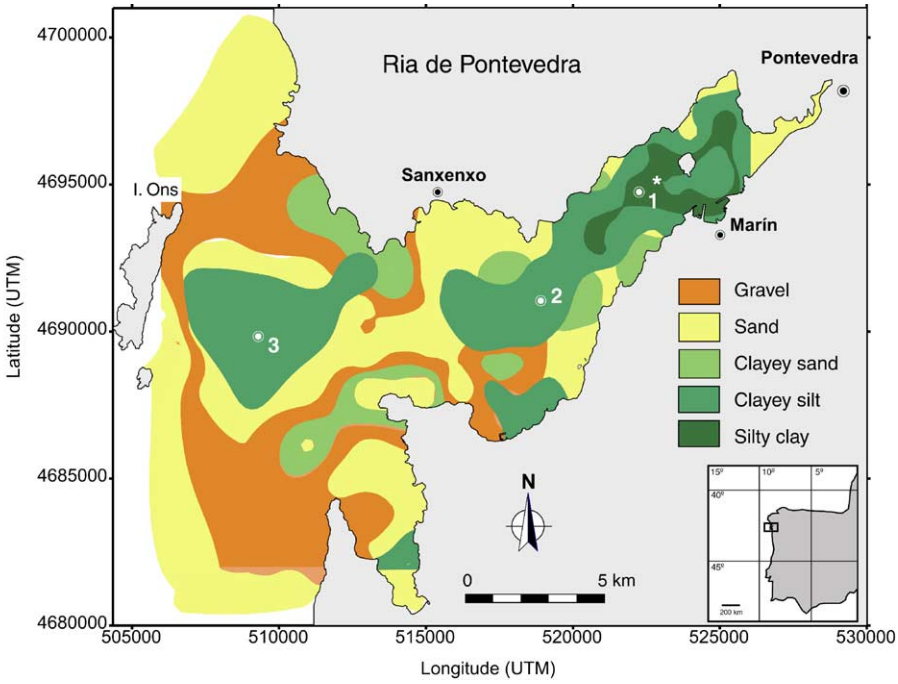

Fig. 1. Sediment distribution along the Ria de Pontevedra (modified after Vilas et al., 1996; Rubio et al., 2001). Locations are also shown for the cores studied (1, 2 and 3).

sedimentation rates and organic matter supply, the major coastal factors that control the geochemical evolution of the sediments are wave climate, coastal morphology and water depth.

Transitional environments like the Ria de Pontevedra on the northwest Atlantic coast of Spain (Fig. 1) provide an exceptionally good opportunity to study sediment diagenesis under a wide range of geochemical conditions, and to test whether the diagenetic signals can be disentangled from inhomogeneities in the source material. The present study aims to explain the effects of these processes on the magnetic properties of the ria sediments and how these hold unique information regarding the post-depositional evolution of coastal sediments. This paper will also explore how magnetic properties help to reveal encrypted forcing mechanisms such as water depth and wave climate, and thus to clarify their role in this type of sedimentary environment.

2. Study area

The Ria de Pontevedra is a funnel-shaped, deep embayment on the southern part of the Galician coast of northwestern Spain (Fig. 1). It is about 30 km long, and has a maximum width of 12 km at its mouth. Its sedimentary dynamics bear some similarities to wave-dominated estuaries, but with less fresh continental water input, and higher primary productivity due to seasonal upwelling (Prego et al., 2001). Average sedimentation rates are about 1 mm yr^{-1} (Rubio et al., 2001). Wave conditions exert an important control on sediment distribution (Vilas et al., in press). Fine-grained and organic-rich sediments accumulate in low-energy areas along the deep central axis, and in protected areas toward the inner part. In contrast, coarse bioclastic, carbonate-rich sediments occur on its margins and on the outer part, where the wave energy is stronger. The waves affect the seabed sediment by periodically remobilizing and oxygenating the top sediment, buffering sulphate reduction and contributing to the formation of authigenic iron oxides by reaction of dissolved iron diffusing upward from anoxic layers below (Rubio et al., 2001). This also appears to contribute to the gradual depletion of organic matter in the fine sediments observed toward the outer areas of the ria mouth.

Preliminary studies in the area (López-Rodríguez et al., 2000; Rey et al., 2000; Mohamed et al., 2001)

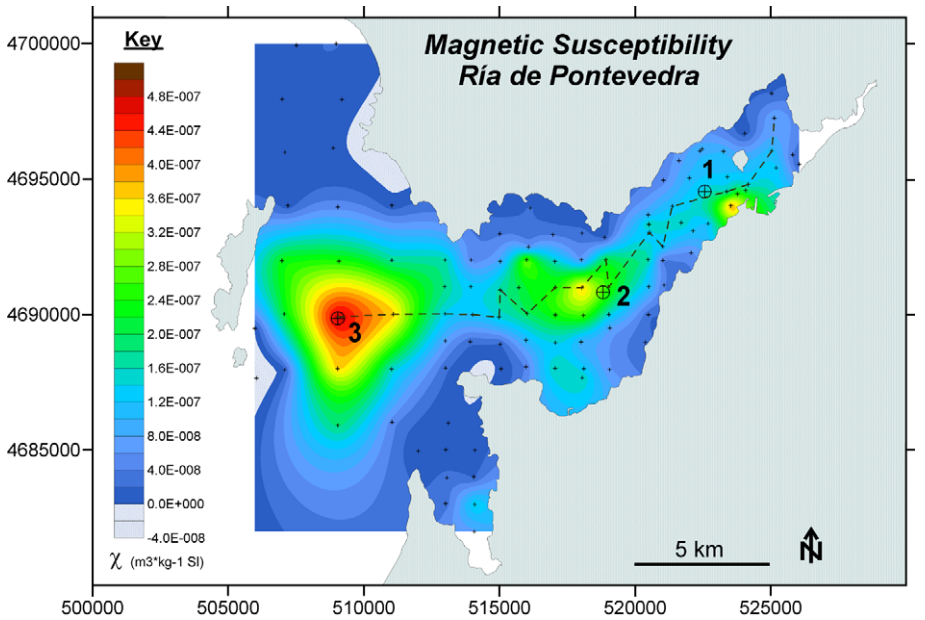

Fig. 2. Magnetic susceptibility (χ) of the surficial seabed sediments of the Ria de Pontevedra. Crosses indicate sample locations. White crosses indicate core positions. The dashed line indicates the trace of the section studied along the central axis of the ria.

pointed out that the surficial sediment distribution of low-field magnetic susceptibility (Fig. 2) can mostly be explained by this textural and hydrodynamic interplay. The increase in diamagnetic carbonate content toward the ria margins, where the coarse material accumulates, results in generally low susceptibility values. The highest values of susceptibility appear along the central axis, where the clay content is high and where carbonate bioclasts are scarce; and toward the outer part of the ria, where oxygenating conditions dominate and favour authigenic formation of Fe oxide and oxyhydroxide. Magnetic susceptibility gradually decreases toward the inner part of the central axis because organic matter decomposition causes reducing conditions. This anoxic/sulphidic environment drives the dissolution of the magnetic oxides and oxyhydroxides that dominate the susceptibility signal in the outer part of the ria.

3. Material and methods

Three gravity cores (between 60 and 90 cm in length) were taken from the inner (core 1), middle (core 2) and outer (core 3) parts of the Ria de Pontevedra along its longitudinal axis (Fig. 1). Each core was sampled at 3 cm intervals using plastic cylinders of approximately 5 cm^3 volume. The remainder of the sediment was saved for textural and geochemical analyses. A further 18 samples were collected from the upper 15–20 cm of the seabed with a shipeck grabber. Part of each sample was saved and stored in 11 cm^3 plastic cylinders after they were open-air-dried. The remainder of the sample was wet-sieved and the <64 μm fraction was retained for separate measurements following a similar procedure. These grab samples were taken along the central axis of the Ria de Pontevedra in order to complete a full transect and to support the geographical validity of the core data.

Several textural and geochemical properties were measured (grain size, total organic carbon [TOC] content, and $CaCO_3$ content, all using standard procedures (Guitián and Carballás, 1976). Elemental analysis was performed by X-ray fluorescence (XRF). Mn speciation was determined by the method of Ure et al. (1993), using acetic acid for exchangeable/carbonate fraction, hydroxylammonium chloride acidified with nitric acid for the oxide/oxyhydroxide fraction and hydrogen peroxide plus ammonium acetate for the organic and sulphidic fraction. Mineralogy was analysed by X-ray diffraction (XRD), and selected samples were also examined by scanning electron microscopy (SEM). A detailed account of the sedimentological and geochemical results from these cores is beyond the scope of this paper, but these data have been presented elsewhere by Rubio et al. (2001). These authors suggested some basic relationships between magnetic susceptibility and key geochemical indicators, which prompted us to pursue further this line of research, by making a more complete set of susceptibility measurements, and establishing the remanence properties of these cores. Their results are used for comparison and are referred to in the discussion of the presented data when necessary.

Magnetic measurements were made of the core samples in plastic cylinders after they were air-dried, and the results expressed on a dry-weight base. Low-field magnetic susceptibility (χ), the coercitivity of remanence (H_{cr}), and S ratios, $S_{-0.1\ T}=-IRM_{-0.1\ T}/IRM_{3\ T}$ and $S_{-0.3\ T}=-IRM_{-0.3\ T}/IRM_{3\ T}$, were calculated for each sample. χ was measured in a Kappabridge, KLY-2 magnetic susceptibility meter and is expressed in mass-specific units ($m^3\ kg^{-1}$). Frequency dependence of susceptibility (χ_{fd}) was calculated as the percentage of measured values at frequencies of 0.74 and 7.40 kHz obtained using a Bartington Instruments MS2B sensor. Isothermal remanent magnetizations (IRMs) were imparted stepwise in a MMPM9 pulse magnetizer in fields up to 3 T. Magnetic remanence was measured using an AGICO JR-5A spinner magnetometer. Anhysteretic remanent magnetizations (ARMs) were measured in a 2G Enterprises cryogenic magnetometer to obtain χ_{ARM} and ARM_{100}/IRM_{100} parameters.

Wave propagation modelling was computer-simulated using the REFDIF Software (GIOC, 1995), which is based on Kirby and Dalrymple (1983, 1985). This tool assumes a refraction–diffraction model that is weakly non-linear, where the wave equation is solved using a third-order Stokes development. This model considers wave shoaling and energy dissipation processes as important elements of wave transformation in shallow water.

Table 1
Bottom shear stresses ($\tau_o=\frac{1}{2}\rho f_w v^2$) computed from the wave propagation numerical model REFDIF (GIOC, 1995)

Core	τ_t	Case 1	Case 2	Case 3	Case 4	Case 5	Case 6	Case 7	Case 8
		$H_o = 2$ $T_p = 12$	$H_o = 2.5$ $T = 14$	$H_o = 3$ $T = 10.5$	$H_o = 3.5$ $T = 11.2$	$H_o = 4$ $T = 12$	$H_o = 4.5$ $T = 12.7$	$H_o = 5$ $T = 13.5$	$H_o = 6$ $T = 18$
1	0.1698	1.8800	2.9370	0.0620	0.0780	0.1182	0.2312	0.4554	1.9300
2	0.1699	0.9655	0.7730	0.0920	0.1055	0.2068	0.1473	0.2776	0.4417
3	0.1707	0.0618	1.0690	0.1218	0.1745	0.1845	0.2148	0.2552	6.8700

τ_t=threshold value for initiation of motion at the studied core sites. τ_o=values calculated for studied cases for the significant wave height (H_o) and peak period (T_p) at deep water. Shaded cells indicate seabed remobilization ($\tau_o>\tau_t$). Shaded areas indicate that the threshold conditions are exceeded.

This type of model is capable of estimating height and direction in an area with irregular bathymetry, and in the presence of obstacles, where diffraction is considerable. The limitation of these models is that they do not take into account wave reflection, which is considered irrelevant to this study. The initial parameters for the propagation model were characterized using the Spanish Port Authority oceanographic database (Ministry of Public Works) that included information from both the Spanish

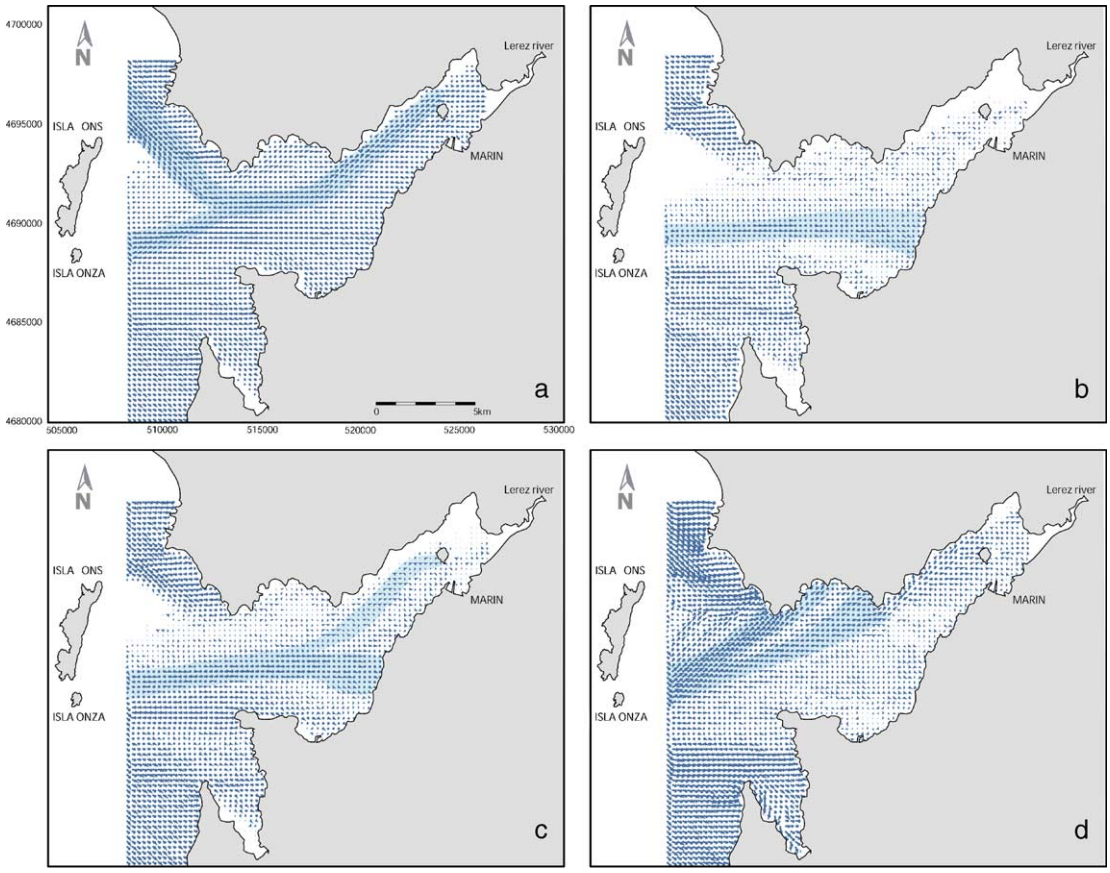

Fig. 3. Numerical simulation of wave propagation showing the wave energy distribution in the Ria de Pontevedra for the most frequent incident direction (NW) and different wave conditions at deep water: (a) H_o=2.5 m, T_p=14 s; (b) H_o=3 m, T_p=10.5 s; (c) H_o=4 m, T_p=12 s; (d) H_o=6 m, T_p=18 s. H_o=significant wave height at deep water and T_p=peak period.

Grid of Measurement and Record of Waves (REMRO) buoys, and the predictive model of wave generation. On the Galician coast, the most frequent wave direction was NW, with average probability of recurrence of 0.46 (168 days yr^{-1}). The simulations were based on a wide range of significant wave heights and peak periods (Table 1; Fig. 3) from the NW, comprising a total probability of around 0.4 (146 days yr^{-1}).

4. Results

4.1. Wave energy

Examples of wave propagation in the Ria de Pontevedra considering different wave heights and peak periods from the NW and a mean tide level are shown in Fig. 3. Arrows indicate wave direction (orientation) and intensity (length). This type of model estimates the wave height from a predefined bathymetric grid. The model results facilitate computation of the wave propagation coefficient (K_p) in the ria interior, which is defined as the ratio between the significant wave height in deep water (H_o), and the significant wave height at a given point (H). The cases studied are given in Table 1.

These results show that the wave distribution pattern in the Ria de Pontevedra is constrained by the presence of the islands of Ons and Onza, which define two entrances at the northern and southern ends of the ria mouth (Fig. 1). The general pattern of wave action shows that the maximum wave energy is concentrated in the outermost exposed areas of the ria. The southern entrance is wider, so wave crests entering this way tend to penetrate deeper into the ria. In general terms, wave energy is smaller in the axial region due to the greater water depth. In the inner part of the ria, the wave energy concentrates in a well-defined corridor, the position of which varies depending on the deep-water wave conditions (see shadow areas in Fig. 3). Such variations are related to the wave peak period (T_p) for each case, as this parameter determines whether the waves propagate from deep to intermediate or shallow-water depths. The longer the period, the deeper the transition. Consequently, the evolution of waves along the ria that are mostly controlled by wave refraction will be constrained ultimately by when and where the waves touch bottom. This pattern is completely consistent with the sediment distribution described in the previous sections: the presence of coarse-grained sediment is greater at shallow depths and toward the open sea, whilst the finer-grained material concentrates at greater depths and toward the inner parts of the ria.

The wave height results, considered along with depth and surficial sediment grain size at the three coring sites, facilitate the estimation of entrainment conditions. Comparison of the threshold shear stress (τ_t), determined from the median grain size of the upper sediment layer (Shields, 1936), and the wave bottom shear stress (τ_0) exerted at these localities (Jonsson, 1966) indicates surficial sediment remobilization for most of the cases studied (Table 2). Furthermore, the results also highlight that the waves' transport capacity is somehow independent of the deep-water significant wave height. Waves of 2.5 m height are capable of mobilizing the sediment at the three sites studied, whilst for 3 m high waves, entrance conditions are not attained at any of the locations. This is mostly conditioned by the position of the wave energy corridors in the inner zone of the ria.

4.2. Magnetic mineralogy determined by SEM and XRD analyses

Initial SEM and XRD analyses identified several mineralogical components that might contribute to the sediment magnetic properties (López-Rodríguez et al., 1999; Rubio et al., 1999, 2001). We present here the results of further work specifically oriented toward the

Table 2
Entrainment conditions for the uppermost sediment of the three cores for case 2

Core	D_{50} (mm)	τ_t	dp (m)	H (m)	τ_o
1	0.01720	0.1698	22	1.05	2.937
2	0.01525	0.1699	35	0.66	0.773
3	0.01340	0.1707	47	1.16	1.069

D_{50}=median grain size calculated from the upper 20 cm of each core. τ_t=threshold shear stress necessary to initiate sediment movement (Shields, 1936). dp=water depth. H=significant wave height in each core location for case 2. τ_o=shear stress reached at the core locations for case 2 (Jonsson, 1966).

identification of magnetically relevant mineral phases. We have identified detrital, authigenic and anthropogenic magnetic phases. The upper 20–30 cm of cores 3 (outer) and core 2 (middle) are dominated by Fe oxides and oxyhydroxides. Detrital minerals like ilmenite and ilmenohaematite occur either as isolated grains (Fig. 4a) or forming part of mud chips (Fig. 4c). Fly ashes (Fig. 4b) occur in a variety of sizes and textures, with variable composition but most are iron-rich. Authigenic goethite has been positively identified in these samples, mainly as partial replacements of shells (Fig. 4e) or other carbonate skeletal parts (Fig. 4f,g). Authigenic Fe sulphides, ranging from monosulphides (Fig. 4d,l) to pyrite (Fig. 4h–j), are widely present in the lowermost part of these cores, and completely dominate core 1 (inner, Fig. 4d). Iron sulphides are also present in the topmost samples of cores 2 and 3, but they are restricted to confined microenvironments like foraminifer tests, where reducing conditions may have developed locally (Fig. 4k).

4.3. Cores geochemistry: Fe, S and Mn with depth

Vertical profiles of total content in Fe, S and Mn for cores 1, 2 and 3 are shown in Fig. 5. Fe and Mn were chosen due to their sensitivity to diagenetic changes and S was chosen as an indicator of organic matter status. In core 1, the near-constant values for Fe and Mn with depth suggest homogeneous negative redox potential values and, therefore, it is unlikely that the surface sediments present suitable conditions for oxidation and precipitation of either Fe or Mn oxides. Hence surface enrichment is not seen at this site. The anoxic/suboxic zone is present from 1 cm below the surface, which leads to the reduction of Mn and Fe oxides and SO_4. In contrast to core 1, cores 2 and 3 show a progressive downward depletion in Fe and Mn from approximately 20 cm depth. The depth of sudden change of Fe and Mn concentrations can be used as a marker of the redox-cline. The higher Fe contents in near-surface sediments in cores 2 and 3 occur at slightly deeper depths than Mn due to the increased sensitivity of Mn to redox change (Cochran et al., 1998). The enhancement of Fe and Mn in estuarine sediments is a well-documented phenomenon (Zwolsman et al., 1993; Valette-Silver, 1993; Spencer, 2002). The reduction of Fe^{3+} and Mn^{4+} results in the mobilization and upward diffusion of these metals to oxic surface sediments where they are re-precipitated either as oxides, or occasionally as carbonates (Farmer and Lovell, 1984). Examples of re-precipitation and replacement by Fe and Mn are common in carbonate bioclasts in cores 2 and 3 (Fig. 4e and f). With burial comes the microbial decomposition of organic material, resulting in the bacterial utilization of O_2 and other inorganic oxidizing agents such as NO^{3-}, MnO_2, $Fe(OH)_3$ and SO_4^{2-} (Froelich et al., 1979; Santschi et al., 1990; Buckley et al., 1995). This is consistent with the low S levels observed in the top 15–20 cm of cores 2 and 3, and its gradual increase with depth (Fig. 5). For core 1, the high content of organic matter caused higher levels of anoxia and, in turn, higher contents of S.

However, diagenetic increase of Fe and Mn may occasionally be masked by grain size, where the use of metal/Al ratios, as a grain size proxy, highlights the diagenetic effect (as can be seen in Fig. 5 for the Fe). For this reason, it is useful to determine the sediment-bound metal phases by sequential chemical extraction (Fig. 6). In core 1, Mn is significantly bound to the organic/sulphidic phase, but in cores 2 and 3 it is mainly bound to oxyhydroxides. This is consistent with stronger reducing conditions in core 1 than in cores 2 and 3. If Mn is available in solution, it may be re-precipitated with calcite at increased alkalinity, which can be confirmed by the higher Mn percentages in the exchangeable/carbonate fraction in cores 2 (28.66%±6.20) and 3 (37.34%±4.21) in comparison with core 1 (12.44%±2.17). Although, in general terms, Mn levels are low, and suggest suboxic conditions in all cores. Similar conclusions were obtained for Fe by Rubio et al. (2001).

4.4. Magnetic properties

For the three cores studied, variation in χ shows a distinctive pattern controlled by water depth and distance of the coring sites to the open sea (Fig. 7a). The highest values in χ occur in the upper part of all three cores. The vertical profiles for cores 2 and 3 then show a marked decrease in χ with depth until a stable value similar for all three cores is reached. In contrast, core 1 has a much flatter profile. The depth at which χ is lowest depends on the core location and increases toward the open sea. Average χ values for

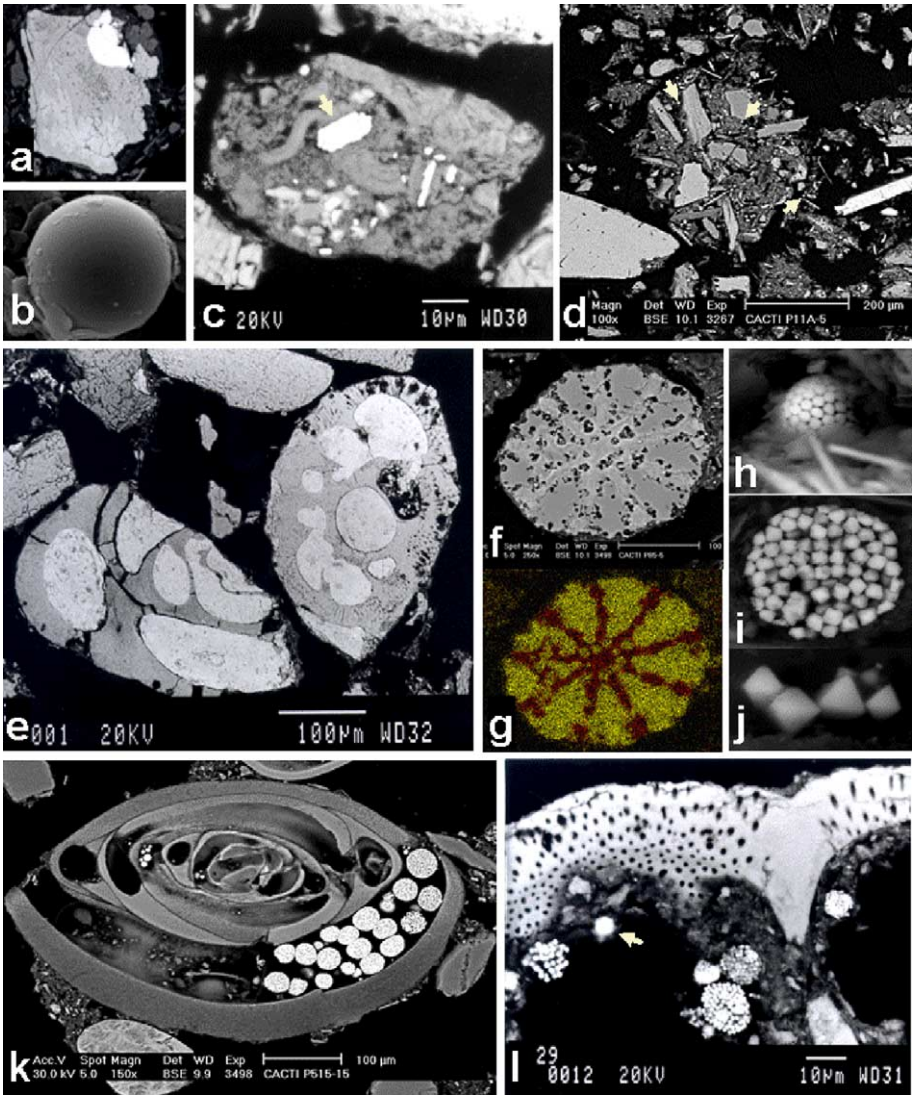

Fig. 4. Electron microscope images of detrital, anthropogenic and authigenic iron oxide phases found in different parts of the Ria de Pontevedra. (a) Typical detrital ilmenohematite showing faint exsolution lamellae. (b) Iron-rich magnetic fly-ash. (c) Mud chip containing small grains of ilmenohematite (arrowed). (d) Typical organic pellet from the internal area of the ria. The numerous small bright dots represent a wide range of iron sulphides ranging from monosulphides to pyrite. Only a few are arrowed. (e) Goethite replacements (bright areas) within foraminifer shells, that are typical of the outer areas of the ria. (f) Partial goethite replacement of a shell fragment (bright area). (g) Color mapping of Fe showing the iron-rich (goethitized) areas in f. (h) Composite pyrite spherule made of small cubic crystals precipitated in clayey sediments of the inner part of the ria. (i) Similar to h, but occurring in the outer areas of the ria, associated with restricted microenvironments within shell interiors. (j) Pyrite may also occur with euhedral octahedral crystal morphologies. (k) Example of extensive pyrite occurrence in restricted microenvironments such as the interior of foraminifer chambers. (l) Detail of the association of several forms of iron sulphides (bright spots and aggregates) occurring in shell interiors and closely connected to organic matter. The arrow points at a monosulphide (Fe:S=1), whilst the more abundant aggregates are typical botryoidal forms form of pyrite (2Fe:S=1). All but b and h (relief) are backscattered electron images of resin impregnated samples. Grey scales and brightness are not comparable between pictures.

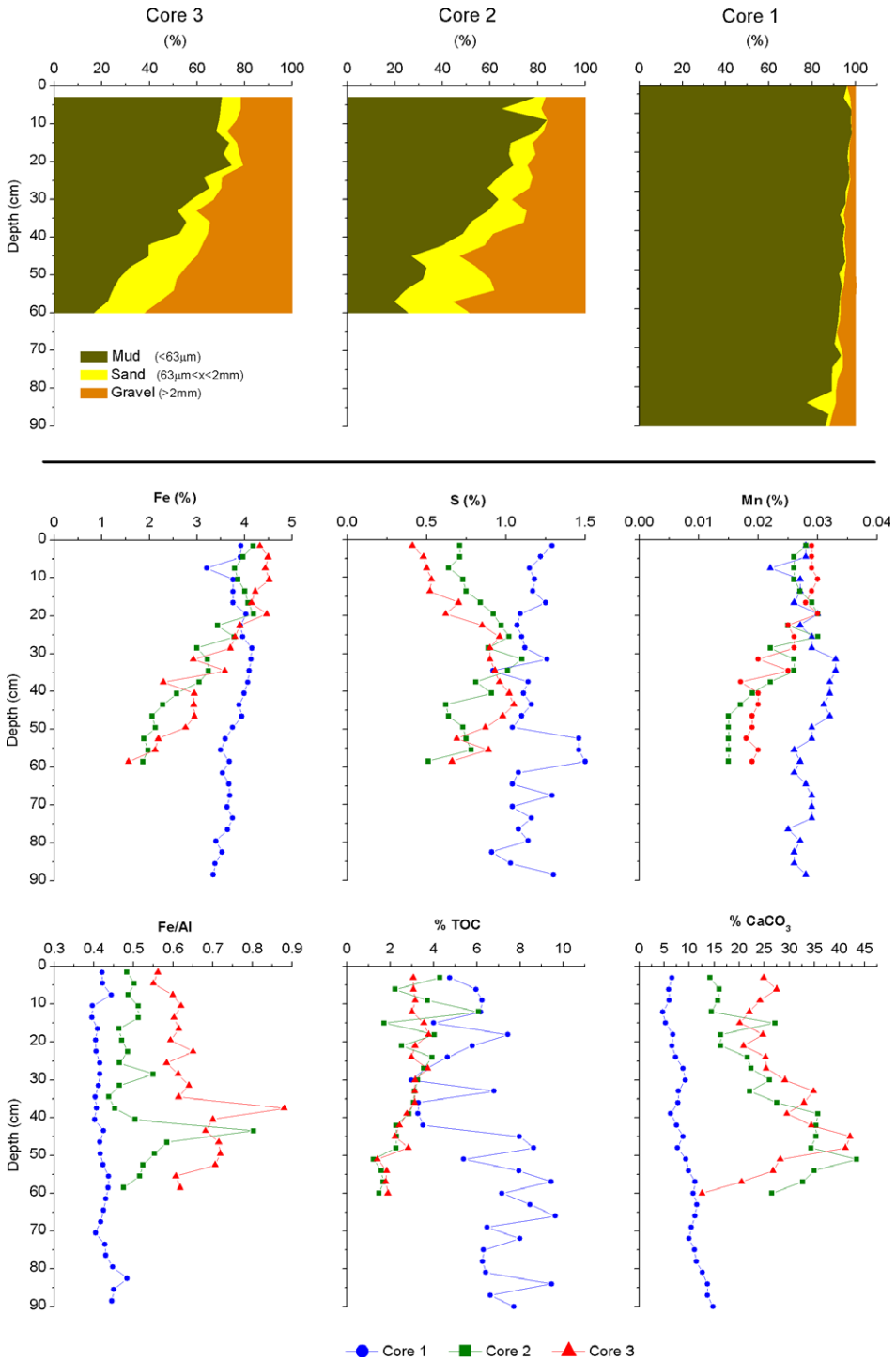

Fig. 5. Sediment grain size, vertical distribution of Fe, Fe/Al, S and Mn (Fe and S, after Rubio et al., 2001) and their corresponding TOC (%) and $CaCO_3$ (%) contents for cores 3, 2 and 1.

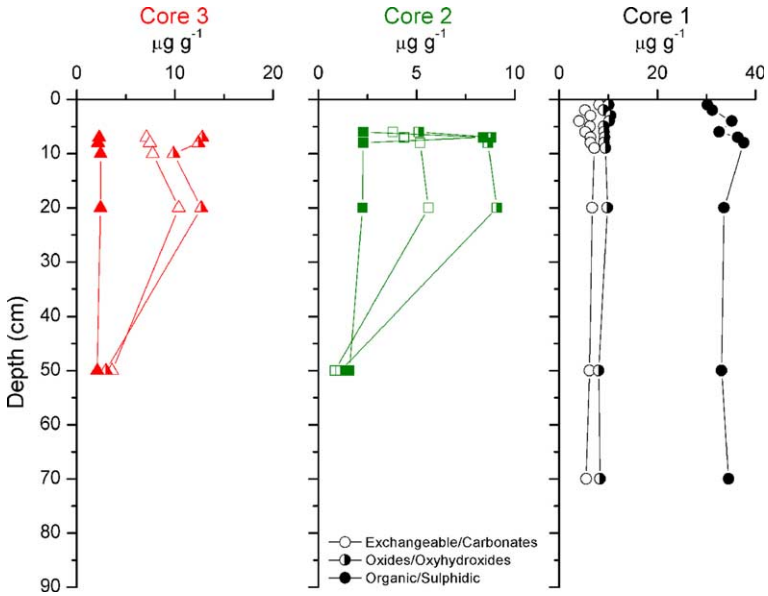

Fig. 6. Sequential extraction for Mn: in exchangeable/carbonate positions, associated with oxides and hydroxides, and bounded to sulphidic/organic phases.

the uppermost high-χ layers also increase toward the open sea.

In a similar fashion, frequency-dependent susceptibility (χ_{fd}) also reflects water depth and distance of the coring sites to the open sea (Fig. 7b). χ_{fd} in the uppermost 15 cm of core 3 (outer) is around 7%, which suggests a significant contribution to χ made by viscous superparamagnetic (SP) grains in this layer. Between 15 and 25 cm there is apparently no SP contribution, with χ_{fd} around 0%. Below 25 cm, the χ signal is so weak that χ_{fd} cannot be reliably determined, and interpretation of χ_{fd} below this depth is not possible. χ_{fd} variations in core 2 (middle) mirrors the behaviour of core 1 but the magnetic signal weakens at a shallower depth. The susceptibility for all of core 1 (inner) is as weak as in the lowest parts of cores 3 and 2, so meaningful χ_{fd} values could not be determined.

χ reflects the bulk concentration of magnetizable material down-core, independently of the grain size of the magnetic components. Magnetic mineral concentrations are higher toward the top of the cores, particularly in the outer areas of the ria. χ_{fd} reflects the concentration of very small superparamagnetic (SP) grains, which have higher concentrations in the upper part of the cores and in sediments from the outer and more marine-influenced areas of the rias.

Variation in magnetic properties provides a fingerprint of the diagenetic processes that lead to the dissolution and precipitation of magnetic minerals at different depths. This is mostly the consequence of organic matter remineralization and wave-related oxygenation, as suggested by the geochemical data. However, full exploitation of the capability of magnetic properties to reveal diagnostic information about how these diagenetic changes take place requires further investigation of the nature and magnetic state of the magnetic phases involved, as revealed by remanence-related properties.

Room temperature remanence properties are good indicators of magnetic mineralogy. Their study allows better definition of their contribution to the observed susceptibility behaviour with depth. IRM acquisition curves for the three cores (Fig. 8) provide useful information regarding the presence and distribution of low- and high-coercivity phases down each core. Three major zones of distinct coercivity behaviour can be identified in core 3. Samples located above 20 cm saturate in relatively low fields (200 mT), indicating that a low-coercivity mineral dominates the observed signal, such as magnetite. Samples located between 20

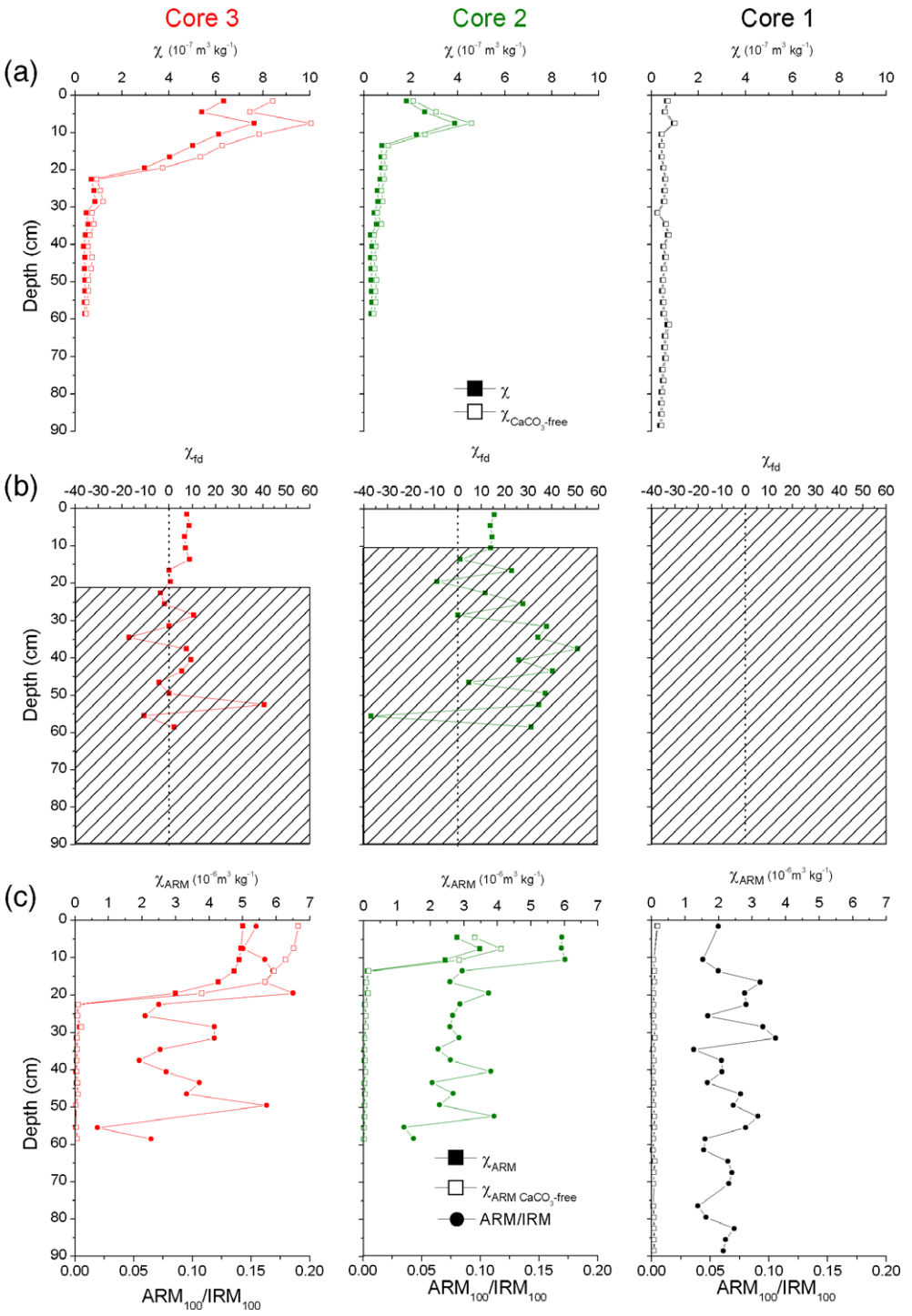

Fig. 7. (a) Magnetic susceptibility variations with depth for cores 1, 2 and 3. Solid squares=bulk susceptibility, open squares=carbonate-free susceptibility. (b) frequency dependence of magnetic susceptibility and (c) susceptibility of anhysteretic remanent magnetization (χ_{ARM}): solid squares=χ_{ARM}, open solid squares=$\chi_{ARM\ CaCO_3\text{-free}}$, circles=$ARM_{100}/IRM_{100}$.

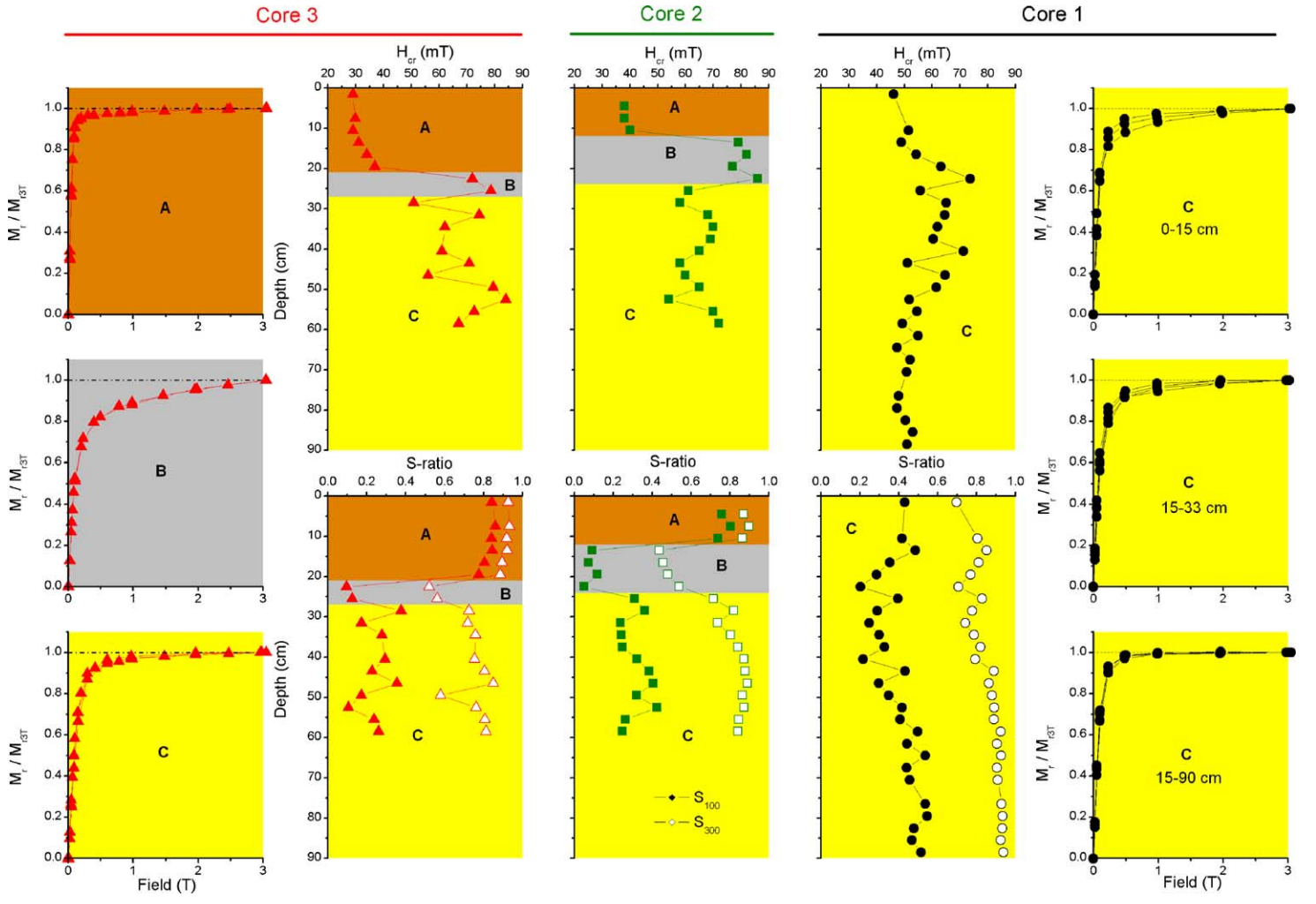

Fig. 8. Remanence properties of studied cores showing their characteristic zonation with depth and distance to the open sea. Isothermal remanent magnetization (IRM) acquisition curves for cores 3 and 1 are normalized to their saturation values (M_r/M_{rs}) and are shown as examples of each zone. Zone A (brown) is dominated by low coercivity magnetite. Zone B (light grey) is dominated by high-coercivity goethite. Intermediate coercivity minerals like greigite and/or pyrrhotite dominate zone C (yellow). (For interpretation of the references to colour in this figure legend, the reader is referred to the web version of the article.)

cm and 30 cm do not saturate at 3 T, indicating the dominance of a high-coercivity mineral such as goethite at this depth. The lowermost samples show intermediate coercivity behaviour, with H_{cr} values of between 100 and 200 mT, suggesting the posibility that ferrimagnetic iron sulphides like greigite and/or pyrrothite make a significant contribution here. IRM acquisition curves for core 2 (not plotted here) can also be grouped in a similar way to those of core 3. In contrast, core 1 does not exhibit this marked zonation with depth, showing coercivity values in the range of the lowermost part of core 3 throughout the whole of the profile (Fig. 8).

Variations in IRM acquisition behaviour facilitated definition of three vertically distinct diagenetic zones (A, B and C) in the three cores. In Fig. 8, each of these zones is characterised by simple parameters derived from the IRM curves, including the coercivity of remanence (H_{cr}) and the S ratios. The H_{cr} parameter is proportional to the magnetic hardness of the sample (coarse-grained magnetite-type behaviour being "soft", fine-grained behaviour being harder, with a haematite/goethite-type behaviour being hardest). The surficial values for H_{cr} are lowest (30–40 mT) in the outermost parts of the ria (core 3). These values increase gradually toward the inner part of the ria (cores 2 and 1). In cores 2 and 3, H_{cr} increases slightly with depth until it sharply increases (80–90 mT) at intermediate depths (12 cm in core 2 and 20 cm in core 3), and decreases again showing a more complex pattern. In contrast, H_{cr} in core 1 increases gradually with depth without any sharp changes, matching the trends observed in the lowermost part of cores 3 and 2.

This magnetic zonation is also supported by the S ratios calculated using both 100 mT ($S_{-0.1\ T}$) and 300 mT ($S_{-0.3\ T}$) reverse fields (Stober and Thompson, 1979; Thompson and Oldfield, 1986; Bloemendal et al., 1988), which are estimates of the relative contribution of soft and hard magnetic phases, respectively. Cores 2 and 3 (Fig. 8) show initial $S_{-0.1\ T}$ and $S_{-0.3\ T}$ values between 0.8 and 0.9. These values are sustained down to a depth of 20 cm in core 3, and only down to 12 cm in core 2 (zone A in Fig. 8). $S_{-0.1\ T}$ and $S_{-0.3\ T}$ values at these depths are similar, supporting the occurrence of a soft magnetic mineral like magnetite as the main remanence carrier. Deeper in cores 2 and 3, $S_{-0.1\ T}$ and $S_{-0.3\ T}$ undergo a sharp decrease to values of 0.1 and 0.6, respectively, which matches the relative H_{cr} increase at those depths. This observation suggests that this part of cores 2 and 3 (zone B) is dominated by a high-coercivity phase like goethite, which is also supported by the XRD data. The S ratios of cores 2 and 3 in zone C increase (Fig. 8), although they do not generally reach the values observed in zone A. The S-ratio behaviour of the whole of core 1 resembles zone C in cores 2 and 3. The variation of $S_{-0.1\ T}$ and $S_{-0.3\ T}$ in core 1 is smooth, showing a slight increasing trend with depth. Differences between surficial ($S_{-0.1\ T}$ around 0.4 and $S_{-0.3\ T}$ around 0.7) and basal samples (S_{100} around 0.5 and S_{300} around 0.9) are small but significant.

This distinct magnetic zonation is also detected in changes of the coercivity spectrum with depth, which can be estimated by the size of the gap between the $S_{-0.1\ T}$ and $S_{-0.3\ T}$ ratios. In summary, 80% of the remanence in zone A (uppermost horizon) is dominated by low coercivity minerals (probably magnetite). In contrast, the remanence at greater depths is dominated by a wider spectrum of coercivities, or at least by two or more populations of minerals with distinct coercivities. In zone B, 10% of the remanence is dominated by minerals with coercivity <100 mT (possibly magnetite), between 40% and 50% of the remanence is carried by minerals with coercivity <300 mT (probably greigite) and about 50–60% of the remanence is carried by minerals with coercivity >300 mT (goethite). In the lowermost zone C, 60–80% of the magnetization is carried by minerals with coercivities <300 mT, but >100 mT, suggesting the occurrence of greigite and/or pyrrhotite. Whilst this zonation is mostly due to the mineralogical composition, intra-zone trends may result from grain size variations.

Finally, χ_{ARM} was used to estimate the contribution of single domain (SD) magnetic minerals (∅ around 0.03 to 0.5 μm in magnetite) with coercivities <100 mT (Fig. 7c). The highest values of χ_{ARM} are found in the upper part of cores 2 and 3, but they decrease with depth until a value close to zero is reached. This indicates the virtual absence of SD minerals in the lowest parts of cores 2 and 3. Only the uppermost sample of core 1 has a χ_{ARM} value above the background level, although even this value is significantly lower than in the uppermost part of the other two cores. These trends and threshold

depths also match the behaviour of χ (Fig. 7a) with depth. This indicates that (a) the depth-decreasing pattern of χ and χ_{ARM} is caused by the same process, and (b) that the major contributor to χ in the upper parts of the three cores are SD minerals and (c) that paramagnetic minerals dominate the background values of χ.

Investigation of concentration independent quotients like ARM_{100}/IRM_{100} (Fig. 7c) provides information about the relative proportion of SD versus multidomain (MD) magnetic grains ($\varnothing$>100 μm) within a magnetic assemblage. For all cores, this parameter follows a general trend consistent with progressive dissolution of small grains, and subsequent relative increase in grain size, which is comparable to the χ and χ_{ARM} trend, but it gives extra information about the low-susceptibility zones identified earlier (Fig. 7). In particular, core 1 reveals a maximum value at ~20 cm, which is followed by a marked drop. This behaviour is repeated quasi-cyclically with peaks at approximately 30, 50, 70 and 90 cm. Similar behaviour is also apparent in the lower parts of cores 2 and 3, and is probably caused by variation in grain size and/or by variation in the proportion of higher-coercivity minerals such as greigite. Roberts (1995) has pointed out that the occurrence of greigite in a SD-like state is typical of anoxic environment; this may be proposed as an alternative explanation for the higher ARM_{100}/IRM_{100} values in this interval. This may be related to dissolution enhancement within layers that produced variations in grain size, or compositional sorting during sedimentation. Magnetotactic bacterial enhancement below redox fronts, a common feature in marine sediments (op. cit.) has also been considered. However, TEM inspection of numerous magnetic extractions and the study of First-Order Reversal Curve (FORC diagrams, Roberts et al., 2000) and Wohlfarth ratios in similar environments of the adjacent rias of Vigo (Mohamed et al., 2004) and Arousa (Emiroglu et al., 2004) showed no positive evidence of their occurrence.

5. Analysis and discussion

Magnetic properties reveal three distinct diagenetically modulated zones in the cores studied. In summary, 80% of remanence in zone A is dominated by ferromagnetic minerals, probably magnetite. In contrast, in zone B, 10% of the remanence is probably due to magnetite, between 40% and 50% is probably due to greigite and about 50–60% by goethite. In zone C, 60–80% of the remanence is probably carried by greigite and/or pyrrhotite. χ_{fd} and χ_{ARM} indicate that this mineralogical zonation is also accompanied by variations in magnetic grain size with a general increase in magnetic grain size down-core, which is also consistent with the H_{cr} and S-ratio profiles which is also accompanied by an increasing proportion of paramagnetic minerals. Further geochemical and mineralogical evidence indicates a slight offset of the Mn and Fe enhancement in zone A of cores 2 and 3, an enrichment trend of S with depth in cores 2 and 3, and widespread precipitation of pyrite in zone C (all cores, but especially core 1). This zonation seems to reflect magnetic grain size and compositional changes resulting from progressive diagenetic modification of the magnetic assemblages, with smaller scale variations probably associated with detrital inhomogeneities within layers. Local wave conditions at the three sites studied effect periodic remobilization and concomitant oxygenation of the upper sediment layers.

5.1. Evidence of diagenesis

Geochemical analyses allowed us to investigate in detail the origin of the observed variations in the magnetic signals of the cores. Textural properties of the sediment did not correlate significantly with any of the magnetic properties, so the observed magnetic variability is not sufficiently explained by changes in detrital input.

The organic carbon content showed a positive correlation with sulphur, similar to what is generally reported in normal marine environments (Berner, 1984). S/C, S/Fe and C/S ratios are generally used to characterize the depositional environment, particularly regarding the presence of O_2 or H_2S.

A S/C ratio of 0.36 is the global average in normal marine sediments (Berner and Raiswell, 1983; Raiswell and Berner, 1986). Samples from cores 2 and 3 have S/C ratios that are close to this value, 0.32 ± 0.11 and 0.30 ± 0.13, respectively. In contrast, samples

from core 1 have S/C ratios of 0.20±0.07, which is well below the reference value. Samples from the upper part of cores 2 and 3 (mostly from zones A and B) have the lowest concentration of both S and C, which correspond to the values reported for magnetite-dominated zones by Kao et al. (2004), whilst all the samples from core 1 and most of the lowest part of cores 2 and 3 (zone C) correspond to values for the greigite-dominated zone of Kao et al. (2004).

Further to this comparison, two of these indicators of diagenesis were plotted against two magnetic properties (Fig. 9). An iron to sulphur ratio was calculated as 2Fe/S. This ratio is based on the stoichiometry of pyrite and approaches unity as pyrite increases in concentration. As pyrite is the end product of suboxic diagenesis at the penultimate stage of sulphate reduction due to bacterial remineralization of organic matter, its presence throughout zone C is a clear indicator of reductive diagenesis.

Low C/S ratios also have been used to indicate an advanced stage of transformation of organic matter, and thus, of diagenetic evolution (Leventhal, 1983; Borrego et al., 1997). 2Fe/S was plotted against χ (Fig. 9a) and C/S against H_{cr} (Fig. 9b). The results for 2Fe/S vs. χ show a strong positive correlation between the two parameters (R=0.9249, Fig. 9a), with high values for the 2Fe/S ratio corresponding to high susceptibility values. Furthermore, the uppermost

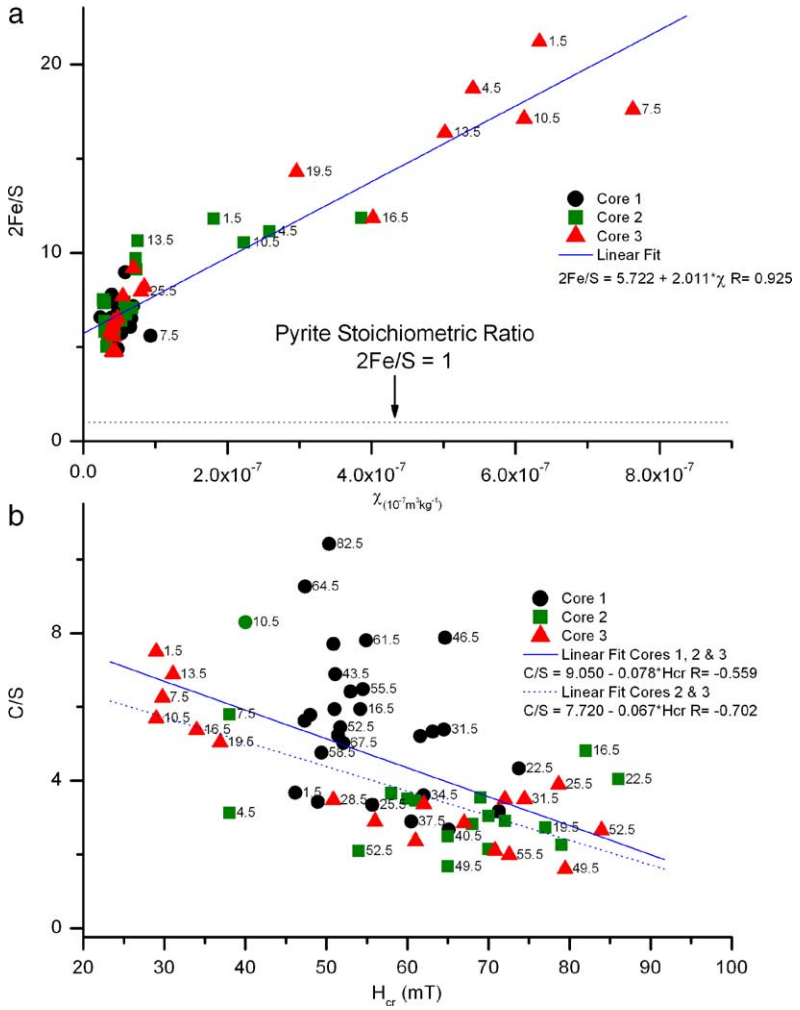

Fig. 9. Comparison of geochemical and magnetic evidence of diagenesis, (a) 2Fe/S vs. χ and (b) C/S vs. H_{cr}.

samples from core 3 have the highest χ values, with those from core 2 showing intermediate values, while lowermost samples from these cores, and all the samples from core 1, exhibit the lowest χ values. This indicates that the processes that are responsible for the decrease in susceptibility are linked to the processes that release Fe, and make it available for pyrite nucleation and crystalline growth, i.e. diagenesis.

C/S also correlates significantly with H_{cr} (R=−0.702, Fig. 9b). In this case, there is a negative correlation with the uppermost samples from core 3 showing the lowest H_{cr} and highest C/S ratios. In core 2, the uppermost samples have intermediate values for both parameters. Samples located at intermediate depths in these two cores have the highest H_{cr} values, and intermediate values for the C/S ratio. For the lowermost samples of these cores, and for all the samples of core 1, this relationship is lost as shown by the poorer correlation (R=−0.559) obtained when results from intensively diagenetically modified core 1 are computed along with data from cores 2 and 3 (Fig. 9b). This indicates that the observed H_{cr} variability in the uppermost zones (A and B) of cores 2 and 3 is affected by diagenesis. As diagenesis progresses, H_{cr} increases up to a maximum value. The increase in H_{cr} is explained by a change in the relative contribution of at least two ferrimagnetic minerals during differential dissolution of magnetic oxides and oxyhydroxides, and during growth of ferrimagnetic iron sulphides as a result of organic matter oxidation. For samples located at intermediate depths, IRM acquisition curves (Fig. 8) indicate that the principal carrier of remanence is a high-coercivity mineral, probably goethite, which was also positively identified by XRD analyses. Below a certain depth, these iron oxide and oxyhydroxide minerals are completely dissolved and a new authigenic mineral, such as a ferrimagnetic iron sulphide, becomes the principal carrier of the remanence. Down-core magnetite dissolution processes are well known in deeper water marine environments. Changes in the relative stability of magnetic phases have also been recently documented in detail for shallower continental shelf marine environments (Yamazaki et al., 2003; Emiroglu et al., 2004). In particular, Liu et al. (2004) describe progressive growth of greigite at depth after the progressive dissolution of hematite and magnetite. The results of Liu et al. (2004) are consistent with those presented here.

5.2. Evidence of wave climate forcing of the diagenetic pathway

The geographic distribution of the three cores studied shows that trends in the magnetic susceptibility (χ) are clearly controlled by distance to the open sea, and core depth. This pattern can be recognised in all of the properties measured. This suggests a strong spatial relationship between depositional processes, sediment particle size and magnetic properties of the sediment. This textural relationship does not exist with sediment depth, which suggests the importance of post-depositional mineralogical transformation of the sediment. Evidence of this textural coupling in surficial samples is presented in Fig. 10, where several textural, geochemical, and magnetic parameters are compared along the ria axis. A gradual increase in susceptibility is evident toward the W, along the central axis of the ria (Fig. 10a and e), which is more evident in the surficial susceptibility data (Fig. 2). This trend is virtually opposite to that exhibited by the trend in sand content (Fig. 10b). This trend is easily explained by the important contribution of diamagnetic biogenic carbonate to the coarse fraction of the sediment due to the high productivity, i.e. shellfish, associated with the observed seasonal upwelling in the area (Vilas et al., 1996). A similar tendency is followed by the TOC (Fig. 10c) which can be mostly explained by textural control of the sediment, as it would normally be expected that coarser sediment would have lower TOC values. Also relevant, in terms of grain size-/composition-related changes, is the opposite trend observed between magnetic susceptibility (χ) and total Fe (Fig. 10d), which also supports the prevalence of post-depositional mineralogical transformations in the sediments.

Considering the above, the magnetic susceptibility of the mud fraction (<64 μm) was measured separately, in order to minimize textural effects caused by the contribution of biogenic carbonate and/or ferromagnetic (s.l.) grains, such as anthropogenic fly ashes or detrital hematite and magnetite, in the coarse fraction (Fig. 10e). Comparison between the magnetic susceptibility of the mud fraction (χ_{mud}, Fig. 10e) and wave energy (expressed as the wave propagation coefficient, K_P) indicates that both increase toward the open sea (W), and are significantly positively correlated (Figs. 10f and 11). These two parameters (K_p

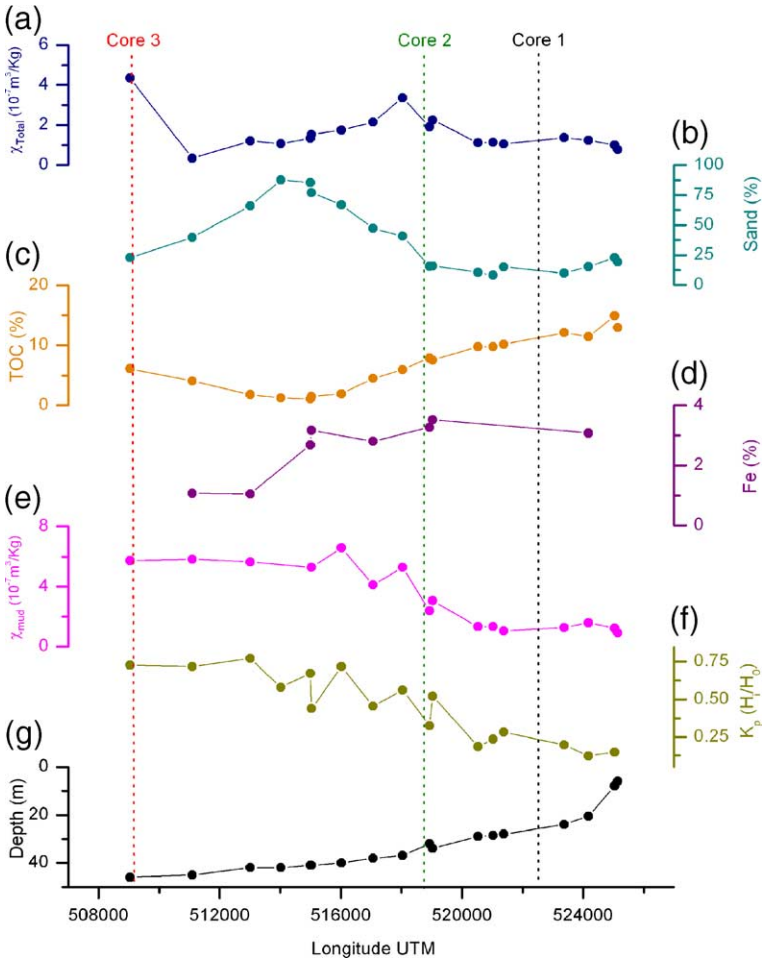

Fig. 10. Longitudinal E–W transect of: (a) magnetic susceptibility of the bulk sample, χ_{total}; (b) percentage of sand; (c) percentage of TOC; (d) percentage of Fe; (e) susceptibility of the mud fraction (<64 μm), χ_{mud}; (f) wave propagation coefficient, K_p, which is an indicator of wave energy; and (g) depth. The profiles are based on 18 samples distributed along the central axis of the Ria de Pontevedra whose location is given in Fig. 2 (crosses joined by the dashed line).

and χ_{mud}) also generally exhibit opposite trends with the TOC content of the sediment and with water depth (Fig. 10g), indicating an association between high mud susceptibility and high wave energy, and greater depth and lower TOC content.

In the broader picture, all of these relationships indicate a general pattern of wave climate forcing of the distribution of coarse carbonate-rich material in shallow waters, which decreases the susceptibility of the sediment by diamagnetic dilution. Wave climate further controls the susceptibility of the mud fraction, independently of the iron content, which superimposes a distinct mineralogical signature that gradually changes toward the west. The early diagenetic evolution of the sediments of the Ria de Pontevedra depends on the upwelling-related organic matter supply, and on wave-climate-related sediment resuspension and associated pore-water oxygenation. It has been demonstrated above that the degree of pyritization and organic C transformation is greater in inner than in outer areas of the ria (León et al., 2004) and that wave energy is higher in the outer areas. Considering these facts, and that seasonal upwelling in the area has a decreasing influence toward the inner part of the ria (Prego et al., 2001), it can be suggested that seabed oxygenation, forced by wave climate

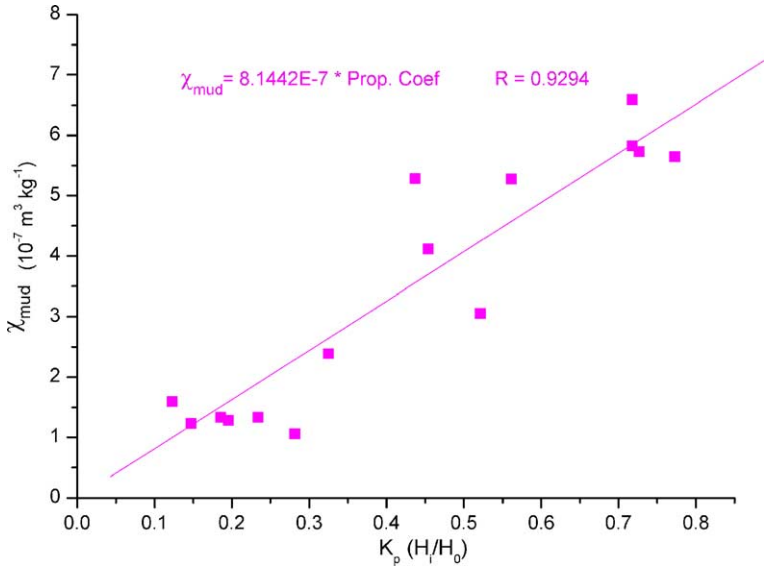

Fig. 11. Correlation between χ_{mud} and wave propagation coefficient, K_p.

remobilization, is the main factor controlling the redoxomorphic diagenesis in the area.

5.3. Hypothesis testing: magnetic susceptibility as a proxy for sediment transport and subsequent diagenetic pathways in the Ria de Pontevedra

This hypothesis has been more strictly tested using the wave propagation model presented earlier. The Shields (1936) diagram predicts larger threshold shear stresses at the sediment/water interface from the inner to the outer part of the ria, as the median grain size within the silt range decreases in that direction. Note that considering the wide range of H_o and T_p values for the ria (Table 2), the conditions required to entrain sediment are exceeded for at least half of the year, which would keep the upper sediment layer well oxygenated. Other important information obtained from these calculations is that wave height does not cause a gradual eastward remobilization of sediments on the sea bottom. Over a given threshold value, seabed remobilization starts everywhere nearly simultaneously.

Once clayey sediments at the three sites have started to move, local sedimentation rates, which mostly depend upon grain size, can easily be estimated from settling velocities (w) following Stokes' law. The settling velocity gradually decreases from the inner to the outer areas according to the median grain size trend (Table 3). However, for the wave action to result in effective resuspension of the unconsolidated sediments on the sea bottom, and for the above calculations to hold, the settling velocity should not exceed the wave shear velocity (u^*), according to the criterion $w<1.25u^*$ (Bagnold, 1956) for suspension. This criterion is satisfied for all three cores (Table 3), which indicates that, for the estimated wave conditions, resuspension will occur most of the year.

Modelling predicts that, under frequent conditions (46% of the time), seabed sediments at the three sites studied is periodically remobilized. However, this

Table 3
Suspension transport and sedimentation conditions for case 2

Core	D_{50} (mm)	dp (m)	w (m/s) (Stokes' law)	u^*	Sedimentation time (St)
1	0.01720	22	0.0002617	0.0028653	23.4 h (1 day)
2	0.01525	35	0.0002057	0.0007541	47.3 h (2 days)
3	0.01340	47	0.0001589	0.0010429	82.2 h (3.4 days)

D_{50}=median grain size calculated from the upper 20 cm for each core. dp=water depth. w (m/s)=fall velocity calculated from Stokes' law as a function of the corresponding D_{50} at this site. u^*=shear velocity calculated for case 2. St=time required for the particles to reach the bottom, and subsequently the time available for OM oxidation.

remobilization trend does not explain the higher degree of oxygenation expected toward more open marine conditions, as suggested by the vertical profile in the magnetic properties of the cores. In contrast, a clearer pattern emerges when calculating the time for a particle to fall to the bottom from the free surface, considering the settling velocity and water depths for each of the cores (Table 3). Sediments located in the inner sector of the ria, with higher settling velocities and a shallower water column to travel through, require less time to reach the bottom than those at the ria's mouth. Consequently, under normal wave conditions, the threshold shear stress for sediments in the ria's middle area is exceeded, and they are simultaneously remobilised. However, during fair weather conditions, local sedimentation rates are much higher in the inner shallow areas than in the outer deep areas of the ria (Table 3). This effect increases by more than three times, the sediment residence time in the water column between the outer (3.4 days) and inner areas (1 day), and provides a likely scenario for the higher degree of water column organic matter oxidation in the outer area. It should be noted that this calculation is an underestimation of the true residence time values, because differences between core 1 and core 3 can easily reach an order of magnitude if both, the tides and the probability of successive periods of bad weather, are also considered. This model is further supported by the significant correlation observed between wave height and clay-fraction magnetic susceptibility (Fig. 11), where low susceptibility and associated highly evolved diagenesis ratios (Fig. 9) correspond to small wave heights and vice versa.

From the above, it can be concluded that the diagenesis pathway in transitional environments depends mostly on the local distribution of wave energy and water depth, rather than on the expected seabed sediment remobilization. Under similar annual to decadally averaged sedimentation rates and organic matter supply, wave climate, coastal morphology and water depth are the major features that control the geochemical evolution of a ria system.

Finally, our results show an important dissociation between spatial distribution in sediment and diagenetic evolution from the typical estuarine-like thermohaline circulation models that are generally proposed for the Galician rias (Gómez-Gesteira et al., 2001; Pardo et al., 2001; Prego et al., 2001; Ruíz-Villareal et al., 2002; Souto et al., 2001; Torres-López et al., 2001). These models explain ria dynamics, as a departure from the classical Dalrymple et al. (1992) model, mostly on the basis of a more open exchange of water masses between the rias and the continental shelf; their associated seasonal upwelling, and their estuarine-like circulation, with modulation by local winds. However, these models fail to explain the observed sediment and organic matter distribution, as proposed by Vilas et al. (1996) and Vilas et al. (in press), and their subsequent diagenetic pathways. The sediment records studied here clearly show textural and hydrodynamic controls that are forced by wave climate, which will ultimately determine key preservation conditions in the sediment record (i.e. strata formation). These distinctive features are alien to estuarine-like environments, and constitute the basis for the long-discussed categorization of rias as a separate sedimentary environment (Vilas in Perillo, 1995; Vilas, 2000, 2002), and could contribute to their potential recognition in the geological record.

6. Conclusions

Magnetic signatures of subtidal sediments investigated in this study are related to their early diagenetic evolution, which is superimposed on a complex interplay between detrital, biogenic and anthropogenic source materials that are forced by wave climate and water depth. Down-core vertical variations in magnetic properties are controlled by the rate of consumption of organic matter and are modulated by small differences in sediment texture. Between cores, variations in magnetic properties are determined by a depth-dependent residence time of TOC in the water column, because frequency of waves causes continuous seabed remobilization and sediment grain size gradation.

In this type of transitional environment, geographically controlled parameters like water depth and wave energy exert a major control over the magnetic properties of the sediments. Magnetic properties therefore cannot be used for short-scale correlation, but they can enable rapid and detailed geochemical characterization, as noted previously by Verosub and Roberts (1995), Dekkers (1997) and Larrasoaña et al. (2003) among others. Once the

relationship between geochemical evolution and magnetic properties is adequately established, magnetic measurements should allow rapid and inexpensive data acquisition in these environments. This is relevant for monitoring and detecting mineralization/mobilization processes associated with pollution, which are especially widespread in coastal ecosystems of high biological productivity and of great economic importance to the Galician rias of northwestern Spain.

The notorious dissociation between spatial sediment distribution and subsequent diagenetic evolution of the sediments, as distinct from the estuarine-like models generally invoked for the Galician rias, supports the categorization of ria-type systems as distinct sedimentary environments. Further studies will enable evaluation of the basis for potential recognition of their associated facies in the geological record.

Finally, magnetic properties have revealed encrypted wave forcing mechanisms that control early diagenesis in this type of environment. For longer sediment cores, they will also provide the basis for estimating the prevalence and temporal scale of such mechanisms, and their possible relationship with millennial-scale climatic changes in the area.

Acknowledgments

We appreciate very much the constructive suggestions from A. Roberts, S. Robinson and Editor De Lange, which greatly improved the paper. This work was funded by projects RTN ERBFRXCT98-0247 (Mag-Net) of the European Union, REN2003-02822 MAR, REN2003-03233 MAR, VEM2003-20093-C03-03 of the Spanish MCYT and PGDIT03R-MA30101PR of the Galician Government (XUGA). Contribution No. 335 of XM2 group (GEOMA).

References

Bagnold, R.A., 1956. The flow of cohesionless grains in fluids. Philos. Trans. R. Soc. Lond. 249 (964), 235–297.

Berner, R.A., 1981. A new geochemical classification of sedimentary environments. J. Sediment. Petrol. 51, 359–365.

Berner, R.A., 1984. Sedimentary pyrite formation: an update. Geochim. Cosmochim. Acta 48, 605–615.

Berner, R.A., Raiswell, R., 1983. Burial of organic carbon and pyrite sulphur in sediments over Phanerozoic time: a new theory. Geochim. Cosmochim. Acta 47, 855–862.

Bloemendal, J., Lamb, B., King, J.W., 1988. Paleoenvironmental implications of rock-magnetic properties of late Quaternary sediment cores from the eastern equatorial Atlantic. Paleoceanography 3, 61–87.

Bloemendal, J., King, J.W., Hall, F.R., Doh, S.-J., 1992. Rock magnetism of late Neogene and Pleistocene deep-sea sediments: relationships to sediment source, diagenetic processes, and sediment lithology. J. Geophys. Res. 97, 4361–4375.

Borrego, J., López, M., Pendón, J.G., Morales, J.A., 1997. C/S ratios in estuarine sediments of the Odiel river-mouth SW Spain. J. Coast. Res. 14, 1276–1283.

Buckley, D.E., Smith, J.N., Winters, G.V., 1995. Accumulation of contaminant metals in the marine sediments with special reference to United Kingdom estuaries: a review. Environ. Pollut. 76, 89–131.

Canfield, D.E., Berner, R.A., 1987. Dissolution and pyritization of magnetite in anoxic marine sediments. Geochim. Cosmochim. Acta 51, 645–659.

Cochran, J.K., Hirschberg, D.J., Wang, J., Dere, D., 1998. Atmospheric deposition of metals to coastal waters (Long Island Sound, New York, USA): evidence from salt marsh deposits. Estuar. Coast. Shelf Sci. 46, 503–522.

Dalrymple, R.W., Zaitlin, B.A., Boyd, R., 1992. A conceptual model of estuarine sedimentation. J. Sediment. Petrol. 62, 113–1146.

Dekkers, M.J., 1997. Environmental magnetism: an introduction. Geol. Min. 76, 163–182.

Emiroglu, S., Petersen, N., Rey, D., 2004. Magnetic properties of sediments in the Ria de Arousa (Spain): dissolution of oxides and formation of sulfides. Phys. Chem. Earth 26, 947–959.

Evans, M.E., Heller, F., 2004. Environmental Magnetism. Principles and applications of enviromagnetics. Academic Press.

Farmer, J.G., Lovell, M.A., 1984. Massive diagenetic enhancement of manganese in Loch Lomond sediments. Environ. Technol. Lett. 5, 257–262.

Frederichs, T., Bleil, U., Däumler, K., von Dobeneck, T., Schmidt, A., 1999. The magnetic view on the marine paleoenvironment: parameters, techniques, and potentials of rock magnetic studies as a key to paleoclimatic and paleoceanographic changes. In: Fischer, G., Wefer, G. (Eds.), Use of Proxies in Paleoceanography: Examples from the South Atlantic. Springer-Verlag, Berlin, pp. 575–599.

Froelich, P.N., et al., 1979. Early oxidation of organic matter in pelagic sediments of the eastern equatorial Atlantic suboxic diagenesis. Geochim. Cosmochim. Acta 43, 1075–1090.

Funk, J.A., von Dobeneck, T., Wagner, T., Kasten, S., 2004. Late Quaternary sedimentation and early diagenesis in the equatorial Atlantic Ocean: patterns, trends and processes deduced from rock magnetic and geochemical records. In: Mutzila, S., Ratmeye, V. (Eds.), The South Atlantic in the Late Quaternary—Reconstruction of Material Budget and Current Systems. Springer-Verlag, Berlin, pp. 237–260.

Gómez-Gesteira, M., DeCastro, M., Prego, R., Pérez-Villar, V., 2001. An unusual two layered tidal circulation induced by

stratification and wind in the Ria of Pontevedra (Spain). Estuar. Coast. Shelf Sci. 52, 555–563.
Grupo de Ingeniería Oceanográfica y de Costas, 1995. Modelo de propagación de oleaje, REFDIF.
Guitián, F., Carballás, T., 1976. Carbonatos y sales solubles. In: Sacro, Pico (Ed.), Técnicas de Análisis de Suelos. Santiago de Compostela, pp. 125–127.
Jago, C.F., Jones, S.E., 2002. Diagnostic criteria for reconstruction of tidal continental shelf regimes: changing the paradigm. Mar. Geol. 191, 95–117.
Jonsson, I.G., 1966. Wave boundary layers and friction factors. Proceedings of 10th International Conference on Coastal Engineering. ASCE, pp. 127–148.
Jouanneau, J.M., Weber, O., Drago, T., Rodrigues, A., Oliveira, A., Dias, J.M.A., Garcia, C., Schmidt, S., Reyss, J.L., 2002. Recent sedimentation and sedimentary budgets on the western Iberian shelf. Prog. Oceanogr. 52, 261–275.
Kao, S.J., Horng, C.S., Roberts, A.P., Liu, K.K., 2004. Carbon–sulfur–iron relationships in sedimentary rocks from southwestern Taiwan: influence of geochemical environment on greigite and pyrrhotite formation. Chem. Geol. 203, 153–168.
Karlin, R., 1985. Geochemical and sedimentological control of the magnetic properties of hemipelagic sediments. J. Geophys. Res. 90, 10373–10392.
Karlin, R., 1987. Authigenic magnetite formation in suboxic marine sediments. Nature 326, 490–493.
Karlin, R., 1990. Magnetite diagenesis in marine sediments from Oregon continental margin. J. Geophys. Res. 95, 4405–4419.
Karlin, R., Levi, S., 1983. Diagenesis of magnetic minerals in Recent haemipelagic sediments. Nature 303, 327–330.
Kirby, J.T., Dalrymple, R.A., 1983. A parabolic equation for the combined refraction–diffraction of Stokes waves by mildly varying topography. J. Fluid Mech. 136, 543–566.
Kirby, J.T., Dalrymple, R.A., 1985. Modification of a propagation model for the combined refraction–diffraction of Stokes waves. Shallow water, large angle and breaking wave effects. Univ. of Florida, Coastal and Oceanographic Engineering, UFL/COEL-85/001.
Larrasoaña, J.C., Roberts, A.P., Stoner, J.S., Richter, C., Wehausen, R., 2003. A new proxy for bottom-water ventilation in the eastern Mediterranean based on diagenetically controlled magnetic properties of sapropel-bearing sediments. Palaeogeogr. Palaeoclimatol. Palaeloecol. 190, 221–242.
León, I., Méndez, G., Rubio, B., 2004. Geochemiocal phases of Fe and degree of pyritization in sediments from the Ría de Pontevedra NW Spain: implications of mussel raft culture. Cienc. Mar. 30 (4), 585–602.
Leslie, B.W., Lund, S.P., Hammond, D.E., 1990. Rock magnetic evidence for the dissolution and authigenic growth of magnetic minerals within anoxic marine sediments of the California continental borderland. J. Geophys. Res. 95, 4437–4452.
Leventhal, J.S., 1983. An interpretation of carbon and sulphur relationships in Black Sea sediments as indicators of environments of deposition. Geochim. Cosmochim. Acta 47, 133–138.
Liu, J., Zhu, R., Roberts, A.P., Li, S., Chang, J., 2004. High-resolution analysis of early diagenetic effects on magnetic minerals in post-middle-Holocene continental shelf sediments from the Korea Strait. J. Geophys. Res. 109 (B3), B03106.
López-Rodríguez, N., Rey, D., Rubio, B., Pazos, O., Vilas, F., 1999. Variación de la susceptibilidad magnética en los sedimentos de la Ria de Vigo (Galicia). Implicaciones para la dinámica sedimentaria y contaminación antropogénica de la zona. Thalassas 15, 85–94.
López-Rodríguez, N., Rey, D., Rubio, B., Vilas, F., 2000. Correlación negativa entre la susceptibilidad magnética y el contenido en metales pesados de origen antropogénico en un medio litoral. Geotemas 1, 111–116.
Mohamed, K., Rey, D., Rubio, B., Vilas, F., 2001. Origen de las variaciones magnéticas en sedimentos de la Ria de Pontevedra (NO de España). Geotemas 3, 215–218.
Mohamed, K., Rey, D., Rubio, B., Vilas, F., 2004. Aplicación de técnicas magnéticas al estudio de alta resolución de sedimentos cuaternarios de la plataforma continental adyacente a las Rías Baixas de Galicia. Geotemas 6 (4), 303–306.
Pardo, P.C., Gil-Coto, M., Pérez, F.F., 2001. Short-time scale coupling between thermohaline and meteorological forcing in the Ria de Pontevedra. Sci. Mar. 65, 229–240 (suppl.).
Passier, H.F., Dekkers, M.J., de Lange, G.J., 1998. Sediment chemistry and magnetic properties in an anomalously reducing core from the eastern Mediterraneam Sea. Chem. Geol. 152, 287–306.
Perillo, G.M.E., 1995. Definitions and geomorphologic classifications of estuaries. In: Perillo, G.M.E. (Ed.), Geomorphology and Sedimentology of Estuaries, Developments in Sedimentology vol. 53. Elsevier, Amsterdam, pp. 17–47.
Prego, R., Dale, A.W., deCastro, M., Gómez-Gesteira, M., Taboada, J.J., Montero, P., Villareal, M.R., Pérez-Villar, V., 2001. Hydrography of the Pontevedra Ria: intra-annual spatial and temporal variability in a Galician coastal system (NW Spain). J. Geophys. Res. 106, 19845–19857.
Raiswell, R., Berner, R.A., 1986. Pyrite and organic-matter in Phanerozoic normal marine shales. Geochim. Cosmochim. Acta 50, 1967–1976.
Rey, D., López-Rodríguez, N., Rubio, B., Vilas, F., Mohamed, K., Pazos, O., Bógalo, M.F., 2000. Propiedades magnéticas de los sedimentos de tipo estuarino. El caso de las Rias Baixas. Cuad. Geol. Iber. 26, 115–126.
Roberts, A.P., 1995. Magnetic properties of sedimentary greigite. Earth Planet. Sci. Lett. 134, 227–236.
Roberts, A.P., Stoner, J.S., Richter, C., 1999. Diagenetic magnetic enhancement of sapropels from the eastern Mediterranean Sea. Mar. Geol. 153, 103–116.
Roberts, A.P., Pike, C.R., Verosub, K.L., 2000. FORC diagrams: a new tool for characterizing the magnetic properties of natural samples. J. Geophys. Res. 102, 28,461–28,475.
Robinson, S.G., 2000. Early diagenesis in an organic-rich turbidite and pelagic clay sequence from the Cape Verde Abyssal Plain, NE Atlantic: magnetic and geochemical signals. Sediment. Geol. 143, 91–123.
Robinson, S.G., Sahota, J.T., 2000. Rock-magnetic characterization of early, redoxomorphic diagenesis in turbiditic sediments from the Madeira Abyssal Plain. Sedimentology 47, 307–394.

Robinson, S.G., Sahota, J.T.S., Oldfield, F., 2000. Early diagenesis in North Atlantic abyssal plain sediments characterized by rock magnetic and geochemical indices. Mar. Geol. 163, 77–107.

Rubio, B., Rey, D., Pye, K., Nombela, M.A., Vilas, F., 1999. Aplicación de imágenes de electrones retrodispersados en microscopía electrónica de barrido a sedimentos litorales. Thalassas 15, 71–84.

Rubio, B., Pye, K., Rae, J.E., Rey, D., 2001. Sedimentological characteristics, heavy metal distribution and magnetic properties in subtidal sediments, Ria de Pontevedra, NW Spain. Sedimentology 48, 1277–1297.

Ruíz-Villareal, M., Montero, P., Taboada, J.J., Prego, R., Leitao, P.C., Pérez-Villar, V., 2002. Hydrodynamic model study of the Ria de Pontevedra under estuarine conditions. Estuar. Coast. Shelf Sci. 54, 101–103.

Santschi, P.H., Höhener, P., Benoit, G., Buchholtz-ten Brink, M., 1990. Chemical processes at the sediment–water interface. Mar. Chem. 30, 269–315.

Scourse, J.D., Austin, W.E.N., 2002. Quaternary shelf sea palaeoceanography: recent developments in Europe. Mar. Geol. 191, 87–94.

Shields, A., 1936. Anwendung der Aehnlichkeitsmechanik und turbulenzforchung auf die Geschiebebewegung. Mitt Preuss Versuchsanstalt fur Wasserbau und Schiffbau, no. 26, Berlin. In German.

Souto, C., Fariña-Busto, L., Álvarez, E., Rodríguez, I., 2001. Wind and tide current prediction using a 3-D finite difference model in the Ria de Vigo (NW Spain). Sci. Mar. 65, 269–276 (suppl.).

Spencer, K.L., 2002. Spatial variability of metals in the intertidal sediments of the Medway Estuary, Kent, UK. Mar. Pollut. Bull. 44, 933–944.

Stober, J., Thompson, R., 1979. Magnetic remanence acquisition in Finnish lake sediments. Geophys. J. R. Astron. Soc. 57, 727–739.

Thompson, R., Oldfield, F., 1986. Environmental Magnetism. Allen and Unwin, London, UK. 227 pp.

Torres-López, S., Varela, R.A., Delhez, E., 2001. Residual circulation and thermohaline distribution of the Ría de Vigo: a 3-D hydrodynamical model. Sci. Mar. 65, 277–289 (suppl.).

Ure, A.M., Quevauviller, P.H., Muntau, H., Griepink, B., 1993. Speciation of heavy metals in soils and sediments. An account of the improvement and harmonization of extraction techniques undertaken under the auspices of the BCR of the Commission of the European Communities. Int. J. Environ. Anal. Chem. 51, 135–151.

Valette-Silver, N.J., 1993. The use of sediment cores to reconstruct historical trends in contamination of estuarine and coastal sediments. Estuaries 16, 577–588.

Verosub, K.L., Roberts, A.P., 1995. Environmental magnetism: past, present and future. J. Geophys. Res. 100, 2175–2192.

Vilas, F. (Ed.), 2000. Geology of the galician rias, J. Iber. Geol. (special issue), 269 pp.

Vilas, F., 2002. Rías and tidal-sea estuaries. Encyclopedia of Life Support Systems. UNESCO-EOLSS (Coastal Zone and Estuaries: Estuarine Systems, 2.6.3.1.). UNESCO.

Vilas, F., García-Gil, E., García-Gil, S., Nombela, M.A., Alejo, I., Rubio, B., Pazos, O., 1996. Cartografía de sedimentos submarinos. La Ria de Pontevedra. Escala 1:50,000. Memoria y Mapas. Xunta de Galicia (in Spanish).

Vilas, F., Bernabeu, A.M., Méndez, G., in press. Sediment distribution pattern in the Rias Baixas (NW Spain): main facies and hydrodynamic implications. J. Mar. Syst.

Yamazaki, T., Abdeldayem, A.L., Ikehara, K., 2003. Rock-magnetic changes with reduction diagenesis in Japan Sea sediments and preservation of geomagnetic secular variation in inclination during the last 30,000 years. Earth Planets Space 55, 327–340.

Zwolsman, J.J.G., Berger, G.W., Van Eck, G.T.M., 1993. Sediment accumulation rates, historical input, postdepositional mobility and retention of major elements and trace metals in salt marsh sediments of the Scheldt Estuary, SW Netherlands. Mar. Chem. 44, 73–94.